

## Impact of parameterizations in snow physics and interface processes on the simulation of snow cover and runoff at several cold region sites

Yongkang Xue,<sup>1</sup> Shufen Sun,<sup>2</sup> Daniel S. Kahan,<sup>1</sup> and Yanjun Jiao<sup>3</sup>

Received 13 November 2002; revised 19 May 2003; accepted 29 May 2003; published 4 November 2003.

[1] A series of numerical experiments have been designed to understand the physics at the soil-vegetation-snow-atmosphere interface and to find the major parameterizations/parameters, which are crucial to simulate cold season processes. Observational data sets from Col de Porte of France, Ovre Lansjarv of Sweden, and Gander of Canada were used to help interpret the results. This study shows that snow layering and compaction are among the most important factors affecting proper simulations of snow depth, snow water equivalent (SWE), surface temperature, and surface runoff. Fixed snow density could produce as high as 100 percent error in estimating snow depth and could cause significant biases in SWE simulation during the melting period. Furthermore, with a bulk snow/soil layer, the simulated surface temperature would persistently be close to the freezing point with substantially hampered variability, and the variability and the amplitude of the runoff during the snow-melting season could also be severely underestimated. The experiments also show that proper snow albedo is crucial during the ablation period and affects the magnitude and timing in both SWE and runoff simulations. Furthermore, this study indicates that the parameterizations in the surface aerodynamic resistance in the stable regime play an important role in determining the sensible and latent heat fluxes during the winter season in the Arctic region and then affect the snow depth simulations and prediction of snow melting as well as runoff timing. Although the snow may fully cover the ground in cold regions during the winter, numerical experiments in this study show the vegetation still exerts a substantial influence in the snow depth and runoff simulations. Numerical experimentation shows that less downward sensible heat on the bare ground produces thick snow cover and extremely high peak runoff, which leads to a typical deforestation scenario in cold regions. *INDEX TERMS:* 0315 Atmospheric Composition and Structure: Biosphere/atmosphere interactions; 1655 Global Change: Water cycles (1836); 1860 Hydrology: Runoff and streamflow; 1863 Hydrology: Snow and ice (1827); *KEYWORDS:* snow parameterization, simulation of snow and runoff

**Citation:** Xue, Y., S. Sun, D. S. Kahan, and Y. Jiao, Impact of parameterizations in snow physics and interface processes on the simulation of snow cover and runoff at several cold region sites, *J. Geophys. Res.*, 108(D22), 8859, doi:10.1029/2002JD003174, 2003.

### 1. Introduction

[2] Snow, one of four components in the cryosphere, plays a crucial role in influencing the variability in the global climate system over a variety of time and spatial scales [Peixoto and Oort, 1992]. Through change of surface albedo and regulation of turbulence heat and momentum fluxes at the surface, snow modifies the exchange of energy between the land surface and the atmosphere and significantly affects the distribution of diabatic heating in the atmosphere. Snow cover is also an effective insulator of the soil thermal column. In addition, snow melting repre-

sents an effective heat sink for the atmosphere and an important source of surface runoff and moisture for the soil.

[3] Due to the importance of snow in the water and energy cycles, in recent years substantial efforts have been made to develop pertinent models to simulate the processes at the soil-vegetation-snow-atmosphere interface. According to the models' complexity, Boone and Etchevers [2001] have divided them into three categories. The first category includes the bucket type of models [e.g., Robock *et al.*, 1995], force-restore type of models [e.g., Pitman *et al.*, 1991; Douville *et al.*, 1995], and single snow layer models [e.g., Verseghy, 1991; Schlosser *et al.*, 1997; Sud and Mocko, 1998; Slater *et al.*, 1998]. The second category consists of schemes with detailed internal snow-processes [e.g., Anderson, 1976; Jordan, 1991; Brun *et al.*, 1992; Lehnings *et al.*, 1998]. These models use multiple snow layers (there could be as many as one hundred layers) and fine temporal scales. The third category of schemes is developed based on the schemes in the second category but with substantial simplifications in physical parameter-

<sup>1</sup>Department of Geography, University of California, Los Angeles, California, USA.

<sup>2</sup>Institute of Atmospheric Physics, Chinese Academy of Sciences, Beijing, China.

<sup>3</sup>University Quebec at Montreal, Montreal, Canada.

izations and layering of snow pack [e.g., *Loth and Graf*, 1993; *Lynch-Stieglitz*, 1994; *Sun et al.*, 1999; *Boone and Etchevers*, 2001; *Niu and Yang*, 2003; *Mocko and Sud*, 2001]. The models in this category are aiming at the applications in global and/or regional models. Studies have shown that the intermediate-complexity schemes have produced better simulations than the simple snow schemes in either off-line mode simulation [e.g., *Jin et al.*, 1999] or coupling with a general circulation model (GCM [e.g., *Stieglitz et al.*, 2001]).

[4] The Project for Intercomparison of Land Surface Parameterization Schemes (PILPS, [*Henderson-Seller et al.*, 1993]) has conducted two model comparison experiments to evaluate the performance of land surface parameterizations with different levels of complexity at high latitudes. In the first experiment (PILPS-2d), 18 years of observed meteorological data from a grassland catchment at Valdai, Russia were used for simulation [*Slater et al.*, 2001]. The results showed that, although the models were able to capture the broad features of the snow regime at both intra- and interannual scales, weaknesses exist, especially in the simulation of early season snow melting events. The possible effects of snow model structure, snow albedo, fractional snow cover, and aerodynamic formulations were discussed as the major factors, which contribute to the scatter in the model simulations. In the second experiment (PILPS-2e) the data sets from the Torne and Kalix River system in northern Scandinavia were used [*Bowling et al.*, 2003; *Nijssen et al.*, 2002]. The results from the PILPS-2e indicated that although participating models captured the broad dynamics of snowmelt and runoff, they had large differences in the simulations of snow accumulation and ablation, turbulence heat fluxes, and stream-flow. *Nijssen et al.* [2002] also found that interpretation of the results was difficult due to different parameterizations in the participating models.

[5] A number of studies have been designed to understand the key processes at the snow-atmosphere interface that have major impact on the snow simulation. For example, *Yang et al.* [1997] and *Lynch et al.* [1998] found that snow albedo and the treatment of partial snow cover caused a large difference in simulations by the Biosphere-Atmosphere-Transfer Scheme (BATS [*Dickinson et al.*, 1993] and other land models. In GCM simulations, *Mocko et al.* [1999] found that separations of temperature prediction and heat capacities of snow from those of ground layers and consideration of the transmission of solar radiation within the snow layer were important to produce proper snow simulations for the Simplified Simple Biosphere Model. *Boone and Etchevers* [2001] compared three snow schemes from the three categories discussed earlier. They found that the inclusion of water retention in an intermediate-complexity scheme (interactions between Soil, Biosphere, and Atmosphere - Explicit Snow, ISBA-ES) caused large differences in simulations of snow water equivalent (SWE) and snowmelt runoff from a simple snow scheme (ISBA-FS, force restore model). On the other hand, differences in modeled SWE between the ISBA-ES and a more complex scheme [*Brun et al.*, 1992] were related to contrasting surface flux parameterizations more than to the internal snow physics. The effect of frozen soil on runoff has also been investigated, but it has been found that this

effect was rather weak [*Pitman et al.*, 1999; *Cherkauer and Lettenmaier*, 1999] or inconclusive [*Luo et al.*, 2003]. Using the Russian soil moisture data, *Xue et al.* [1996b, 1997] found that parameterizations of soil hydraulic conductivity under freezing conditions and specification of soil properties could have an impact on cold region simulations.

[6] In this paper, we further investigate the parameterizations and parameters that are crucial for simulations of snow. By using one host-biophysical model with different snow schemes and parameterizations, and comparing the simulated results with observational data, this study will not only help us to understand the mechanisms governing the water and energy budget in the cold season, but will also shed light on which parameterizations may be more appropriate for snow and runoff simulations. This study should also yield useful information for future field measurement design.

[7] A biosphere model, Simplified Simple Biosphere Model (SSiB [*Xue et al.*, 1991]), and an intermediate complex snow model, Simple Snow-Atmosphere-Soil Transfer model (SAST [*Sun et al.*, 1999]) are employed for this study. The snow scheme of SAST has been coupled with SSiB [*Sun and Xue*, 2001] to enhance SSiB's simulation for the cold season. Please note that in this paper, coupling refers to the coupling between the biophysical model and the snow scheme unless otherwise specified. Since the original SSiB has a simple snow scheme, the intercomparisons between the original SSiB and the enhanced SSiB (both have the same biophysical model but with different snow schemes) reveal the role of snow parameterizations. The major differences in these two schemes, which cause the most important simulation differences, are discussed. Furthermore, a series of sensitivity studies using the enhanced SSiB has been conducted to further test the role of parameterizations in snow/atmosphere interactions and to identify the key processes that may be crucial for snow simulations.

[8] Although it is well known that vegetation cover has an important impact on the warm season water and energy budgets at the land surface and atmosphere, its role in the cold season has not been extensively tested. In this study, we also design sensitivity studies to investigate the impact of land cover change on the water- and energy-related processes in the cold season, in which the available net radiation, which is largely controlled by downward long-wave radiation and snow albedo rather than available water, limits latent heat [*Bowling et al.*, 2003].

[9] Several data from different locations are applied for this study. They include the data from Col de Porte in France, Gander in Canada, and Ovre Lansjarv in Sweden. All these data are from cold regions with either snow depth and/or runoff for validation. Col de Porte data also include measured surface temperature.

[10] In this paper, section 2 briefly introduces the models and the coupling strategy. Section 3 presents several data sets for this study. Section 4 describes the numerical experiments in this study. We first discuss the effect of snow physics and snow albedo using the Col de Porte data and the Gander data. It is followed by discussions of the experiments that examine the role of the parameterization of eddy transfer and melting snow albedo using the Ovre Lansjarv data. Finally, the land cover effect in the Ovre Lansjarv

simulation is also discussed. Our conclusions are then summarized in section 5. We reserve a brief description of the coupling methodology of SSiB/SAST snow scheme for the Appendix.

## 2. Model Description

### 2.1. SSiB

[11] The SSiB is a biophysically-based model of land-atmosphere interactions and is designed for global and regional studies. The model is intended to realistically simulate the controlling land-surface processes and to provide fluxes of radiation, momentum, sensible heat and latent heat to general circulation models and regional models. It consists of three soil layers and one vegetation layer. The model predicts soil wetness ( $W_1, W_2, W_3$ , the fraction of soil water content relative to saturation) for three soil layers; temperatures of the canopy ( $T_c, K$ ), near-surface soil layer ( $T_{gs}, K$ ), and deep-soil layer ( $T_d, K$ ); snow depth on the ground ( $W_g, m$ ), and intercepted water on the canopy ( $W_c, m$ ). *Deardorff's* [1977] force-restore method is used to predict the surface and the deeper soil temperatures. In the soil model, water movement is described by a finite-difference approximation to the diffusion equations. The soil layers receive water from precipitation and melting snow, and they provide water for evaporation from bare soil and transpiration from the canopy. Surface runoff ( $R_{off}, m$ ) and drainage ( $R_{dra}, m$ ) are produced in the surface soil layer and bottom soil layer, respectively. In addition, each soil layer produces runoff whenever it is saturated. SSiB describes the vegetation complex of 12 biomes [Dorman and Sellers, 1989], each of which represents some averaged (typical) soil and vegetation characteristics.

[12] The aerodynamic resistance controls interaction between the vegetated surface and the atmosphere. The equations for heat flux transfer in SSiB are

$$\lambda E = \frac{\rho C_p}{\gamma} \frac{U_*}{C_{TN}^{-1} + C_{TT}^{-1}} (e_m - e_a) \quad (1)$$

for latent heat flux and

$$H = \rho C_p \frac{U_*}{C_{TN}^{-1} + C_{TT}^{-1}} (T_m - T_a) \quad (2)$$

for sensible heat flux ( $W m^2$ ), where  $\lambda$  is latent heat of evaporation ( $J kg^{-1}$ ),  $E$  is evaporation rate ( $kg m^{-2} s^{-1}$ ),  $\rho$  is the air density ( $kg m^{-3}$ ),  $C_p$  is the heat capacity ( $J m^{-2} K^{-1}$ ),  $\gamma$  is psychrometric constant ( $mb K^{-1}$ ), and  $U_*$  is friction velocity ( $m s^{-1}$ ).  $T_m(K)$ ,  $e_m$ ,  $T_a$ , and  $e_a$  are the temperatures and water vapor pressure at the reference height and canopy air space, respectively. Similarity theory [Paulson, 1970; Businger et al., 1971] is used to calculate the aerodynamic resistance ( $C_{TN}^{-1}$  and  $C_{TT}^{-1}$ ) from the canopy to the reference height.  $C_{TN}$  is the neutral heat transfer coefficient and is controlled by the vegetation height, surface roughness length, and reference height. The non-neutral part,  $C_{TT}$ , is determined by the atmospheric stability conditions. Some adjustments based on the vegetation conditions are also included [Xue et al., 1991, 1996a].

[13] The original SSiB has a simple snow package. It characterizes the precipitation as snow that accumulates when the surface air temperature is below freezing. Snow can be accumulated on both the canopy and the ground, which would in turn affect the surface albedo. The downward short-wave radiation is attenuated through the canopy with multiple scattering between canopy and ground. When snow exists, an empirical relationship has been used to establish the relationship between snow depth and snow coverage. The multiple scattering between snow layers on the canopy and snow layers on the ground is included in the model, but the ground snow pack is considered as a bulk layer and the attenuation of radiation within the snow layer is ignored. Snow albedo is related to the snow coverage and solar zenith angle. The aging effect of snow albedo is not taken into account. During the snow melting processes, the snow albedo is adjusted empirically to 60% of the fresh snow albedo. The surface roughness is also modified under snow conditions. However, the snow density is assumed fixed, i.e.  $0.2 g cm^{-3}$ . The emissivities of vegetation and snow for long-wave radiation are assumed to be one.

[14] Snow melting and freezing are also taken into account in SSiB. If canopy/ground temperature is below freezing, melting water and the water stored in the canopy is frozen and accumulates there. If canopy/ground temperature rises above freezing, accumulated snow begins to melt. The melted water becomes runoff. This simple snow sub-model has been tested using observational data [e.g., Robock et al., 1995; Xue et al., 1997; Schlosser et al., 1997].

### 2.2. Coupled SSiB/SAST Snow Scheme

[15] The snow package in the SAST model has been introduced into the SSiB [Sun and Xue, 2001]. The layering scheme is a critical part in the SAST model. After an extensive investigation, it was found that three layers with an appropriate layering scheme were adequate for most cases. Preliminary testing using several snow data showed the three-layer model was able to produce reasonable and consistent results [Sun and Xue, 2001]. In the coupled SSiB/SAST snow package, we fix the layer number in SAST to three rather than varying with the snow depth to save computing time in the GCM and regional models. When the total snow depth becomes less than 5cm, the original SSiB snow scheme is adopted.

[16] There are three prognostic variables in the SAST snow package: specific enthalpy, snow water equivalent, and snow density. Specific enthalpy ( $H1, H2$ , and  $H3$  for three snow layers,  $J m^{-3}$ ) is used in the energy balance equation. The enthalpy of melting water is defined as a reference value ( $=0.0$ ). Therefore, the enthalpy value carried by meltwater drainage and/or infiltration into the underlying snow or soil layer or runoff is always zero. In this way, the energy balance equation can be formulated more precisely and concisely without complicated adjustment for melting water flow, leading to a simpler program and computational efficiency. In the surface energy budget, snow is not considered as opaque to short-wave radiation; rather, the radiation flux intensity decreases according to Beer's law. The short wave radiation flux,  $R_{sw}$  at the snow layer is

$$R_{sw}(Z) = R_{sw}(0) \times (1 - \alpha) \times EXP(-\kappa Z) \quad (3)$$

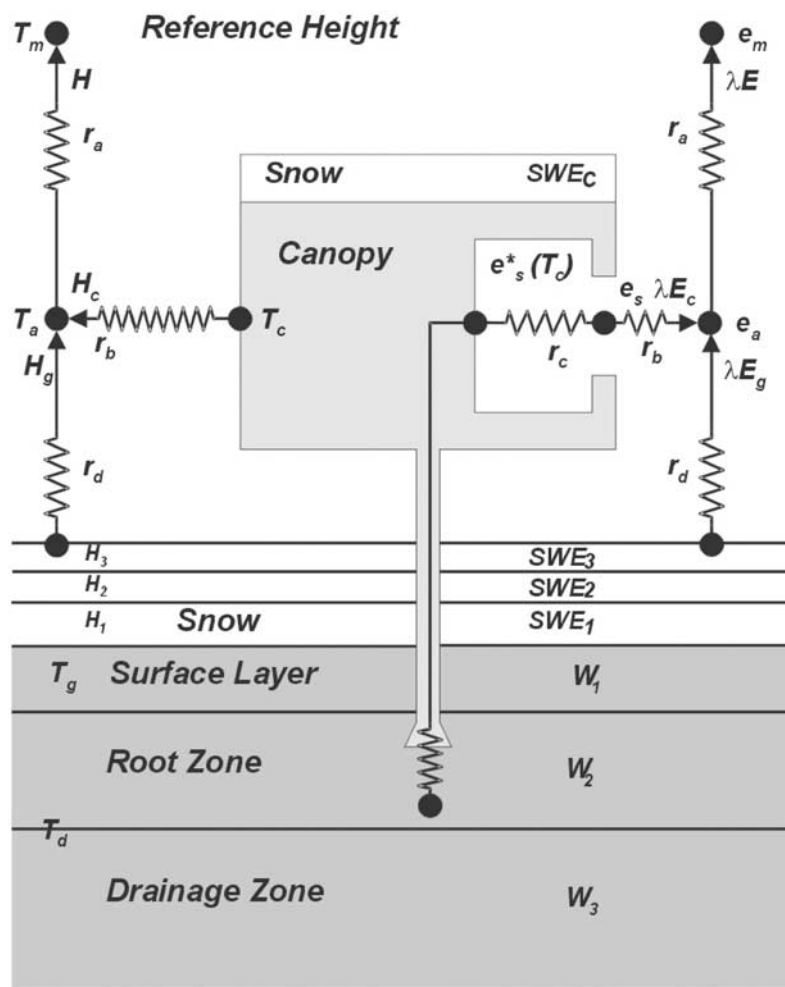


**Figure 1.** Schematic diagram of SSiB/SAST 3-layer snow scheme. The transfer pathways for latent heat and sensible heat fluxes are shown on the left- and right-hand sides of the diagram, respectively. The variables are defined in the text.

where  $\alpha$  is surface albedo,  $R_{sw}(0)$  is short wave radiation at the top of the snow ( $\text{w m}^{-2}$ ), and  $\kappa$  ( $\text{m}^{-1}$ ) is the extinction coefficient to solar radiation. Snow depth ( $Z$ , m) increases in the down direction.

[17] The mass balance describes the changes of snow water equivalent, which is the sum of liquid water and ice grain mass. Since the contribution of water vapor diffusion and its phase change to mass distribution is neglected, snow mass only changes with snowfall and rainfall, snow melting, runoff, and evaporation at the snow surface. Each sub-layer is able to store liquid water content up to a threshold value. Outflow flux occurs when the total amount of liquid water in each layer is larger than the threshold value.

[18] The compaction processes determine snow density and therefore the depth. The compaction includes three components: destructive metamorphism (mainly for new snow), densification process due to snow load or overburden, and snow melting. These three components are determined based on parameterizations [Sun *et al.*, 1999].

[19] In the coupled model, the snow parameterizations for the canopy are kept the same as in the original SSiB, but the

one-layer snow scheme on the ground in SSiB is replaced by the SAST snow scheme when the snow depth is larger than 5cm. To ensure energy conservation in the interaction processes, the prognostic equations of snow entropy and surface soil temperature are solved simultaneously with a backward numerical scheme (Appendix). Energy and water balances are checked at every time step. The snow-covered surface albedo is still calculated by the SSiB's snow albedo package. Figure 1 shows the schematic configuration of the interactions and relations between different components.  $e_m$  (Pa) and  $e_a$  (Pa) are water vapor pressure at the reference height and at the canopy air space, respectively. In addition to aerodynamic resistance between the canopy air space and the lowest atmospheric model layer ( $r_a$ ,  $\text{s m}^{-1}$ ), which is traditionally the only resistance in the surface layer in atmospheric models, SSiB also includes the aerodynamic resistance between the ground surface and the canopy air space ( $r_d$ ,  $\text{s m}^{-1}$ ), and the resistance between the canopy and canopy air space ( $r_b$ ,  $\text{s m}^{-1}$ ), and the stomatal resistance ( $r_c$ ,  $\text{s m}^{-1}$ ) control evaporation from the soil and transpiration from the canopy, respectively. These parameters determine the flux exchange at the surface, and the surface

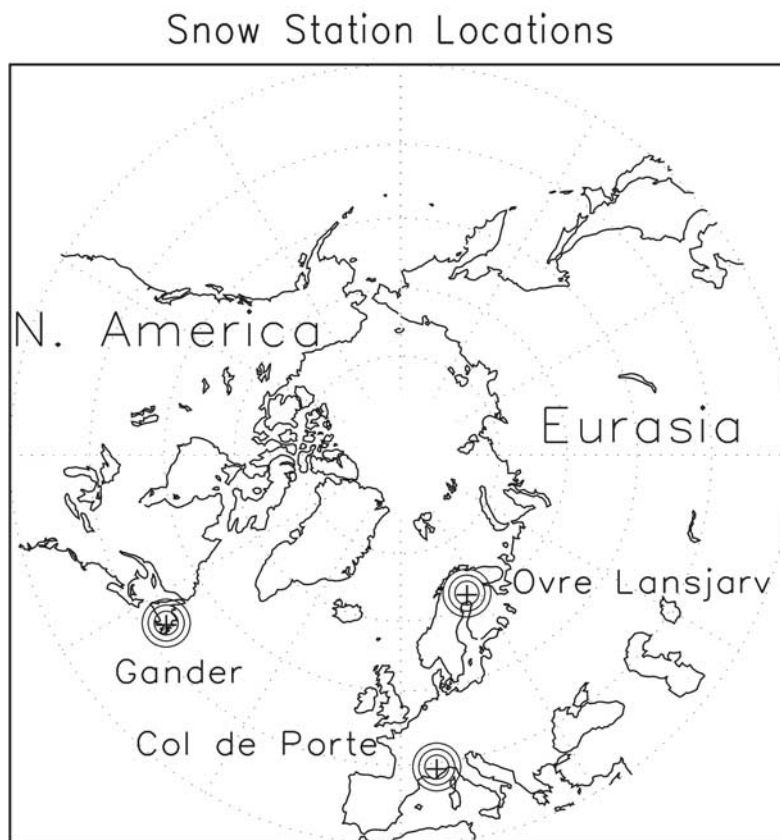


Figure 2. Measuring stations used for this study.

energy partitioning into sensible heat ( $H_c$ ,  $H_g$ , and  $H$ ,  $w m^{-2}$ ) and latent heat fluxes ( $E_c$ ,  $E_g$ , and  $E$ ,  $w m^{-2}$ ).

### 3. Data Set

[20] Several data sets are used for this study. We mainly use two comprehensive data sets. One is from Col de Porte (45°N, 6°E, 1320m) in the French Alps, operated by the Centre d'Etude de La Neige in Grenoble, France. This site is characterized by continuous snow cover in winter, usually from late fall (November to December) to late spring (early May). Air temperatures well above or below the freezing point occur intermittently, so both rain and snow as well as snow melting and refreezing occur during the winter. The land cover is grass vegetation and some relatively tall trees at the edge of the measurement site with loamy soil. All the atmospheric forcing variables were measured hourly at the site. In addition to the meteorological data, the snow depth and surface temperature were measured. The data set covers December to May for 1988–1989, 1993–1994, and 1994–1995. Only the 1994–1995 dataset provided runoff measurements. The snow depth data were taken hourly from ultrasound measurements. The site also had weekly snow pit measurement for SWE and density. However, these measurements were not provided for this study. Some discussions based on the SWE figures in *Boone and Etchevers* [2001] will be presented.

[21] Another data set (the Ovre Lansjarv data) is part of the data used from the PILPS experiment 2e, which vali-

dated models' simulations using measurements that covered the Torne/Kalix River system in northern Scandinavia, which covers about 58,000 km<sup>2</sup> from 65.8 N to 69.1 N and from 18.1 E to 25.1 E. In this Arctic area, the precipitation is characterized by an increasing gradient with elevation: from approximately 1,600 mm year<sup>-1</sup> at high elevation to 500 mm year<sup>-1</sup> over the basin. Annual average temperature varies between 1°C in the south and -3.5°C in the north, and the average number of days with snow cover ranges between 176 and 225 days [Carlson, 1999]. For this study, we only use the data from one sub-basin, Ovre Lansjarv, which lies in Sweden at 66.5813°N, 22.3117°E, just north of the Arctic Circle. It covers an area of 1341 km<sup>2</sup> at an average elevation of 90 m. Different from Col de Porte data, there are a total of ten sites (grid points) in this basin with different vegetation and soil conditions. The primary vegetation in this area is woodland, with some wooded grassland. Lakes cover less than one percent of the area. The primary soil type is sandy loam. Only total river runoff data for this basin were measured, and the data cover the period of 1979–1998. Most of the meteorological forcing data were provided by the Swedish Meteorological and Hydrological Institute [Bowling *et al.*, 2003], but the incoming solar radiation and long-wave radiation were calculated based on the temperature, humidity, and clouds. The wind speeds were taken from the daily surface wind fields of the NCEP/NCAR reanalysis [Kalnay *et al.*, 1996].

[22] In addition, a Gander (Newfoundland, 48.57°N, 54.34°W) data set was also used for model validation to

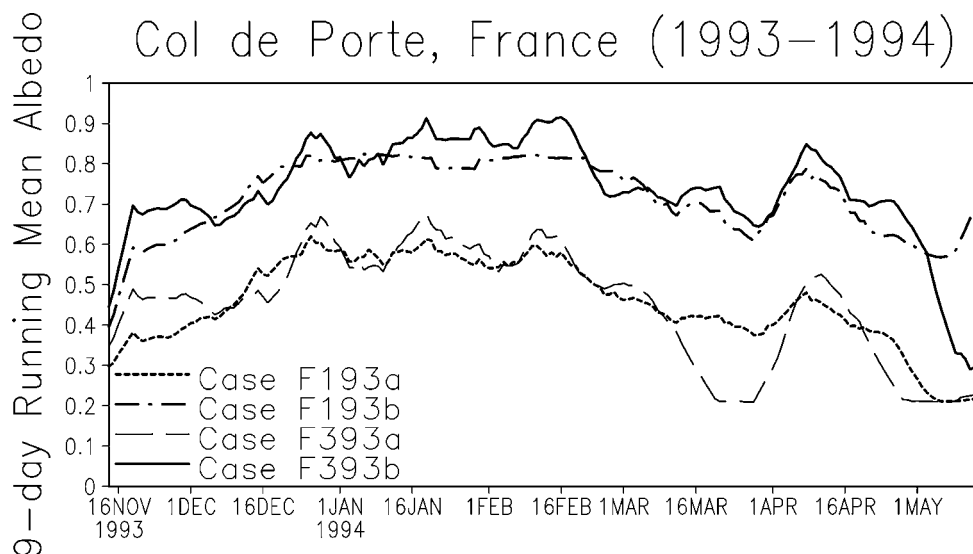


**Figure 3.** The 9-day running mean surface albedo simulated by Cases F193a,b (1-Layer Model), F393a,b (3-Layer Model).

confirm our conclusions from other data sets. This is a lowland station close to the sea at the mid-latitudes. The climate is characterized by the activity of cyclones. At this location, maritime conditions dominate the snow development. From October to April the type of precipitation can either be snowfall or rain. Compared with other lowland conditions at mid-latitudes, Newfoundland has a relatively high precipitation rate due to frequently occurring maritime air masses [Loth and Graf, 1996]. Snow depth is the only variable measured for validation. Because there was no radiation data in the forcing data, we used both reanalysis data and R. Pinker of the University Maryland's radiation data for forcing. Both data produced very similar results. The locations of these three sites are shown in Figure 2.

#### 4. Simulations

[23] We have designed a series of experiments to understand the processes at the snow/atmosphere interface and to examine how the parameterizations influence these processes. From these experiments, we found that snow layering, snow albedo, snow albedo in the melting process, and atmospheric stability conditions have a major impact on our snow and runoff simulations. We will first present the results using Col de Porte data, and then the results using the Ovre Lansjarv data.

##### 4.1. Testing Using the Col de Porte Data

[24] The observational data from Col de Porte, France were used to drive the original SSiB (referred to as 1-Layer model) and the coupled SSiB/SAST snow package (referred to as 3-Layer model). The data covered December 17, 1988 to May 8, 1989, November 10, 1993 to May 20, 1994, and December 17, 1994 to May 20, 1995. The observed conditions were used to specify the initial variables in the model run, and grassland was specified as the land cover. The data from 1993 to 1994 were first used to calibrate the model. The results from the simulations are referred to as

Case F193 for the 1-Layer model and Case F393 for the 3-Layer model.

[25] The fresh snow albedo was about 0.6 in the 1-Layer model, but *Boone and Etchevers* [2001] showed that the observed snow albedo was between about 0.7–0.9 between December 1994 and February 1995. Because of the importance of the snow albedo, to isolate its effect, we set fresh snow albedo to 0.6 (for Case F193a and Case F393a) and 0.85 (for Case F193b and Case F393b), respectively. The variations of the surface albedo for these cases are shown in Figure 3.

[26] Figure 4a shows the simulated snow depths for these four cases. The snow started to accumulate in December and January and the first major ablation occurred in March. During the December and January accumulation processes, there were many variations representing many short melting and refreezing episodes. In early April, the snow started to accumulate again but the ablation process soon kicked in, which led to a complete melting. Before the end of December and after April 1, when the snow depth was less than 1m, the results of the four cases were similar and were close to the observations. However, in both Case F193a and Case F193b (referred to generally as Case F193), snow depth was continually increasing in December and January, and no short melting episodes appeared during this time period. The simulation in early season ablation events has been identified as a major problem in the snow simulation in the PILPS-2d experiment [Slater *et al.*, 2001]. Between January and March, Case F193 produced very high snow depth during the winter season, which was partially caused by the missed melting in December and early January, with less variability than observations. With realistic snow albedo, the snow depth in Case F193b was almost doubled. The correlation coefficients between observed and simulated snow depth were 0.91 and 0.67, and the root-mean-square (RMS) errors of the simulation were 0.64 m and 1.33m for Case F193a and Case F193b, respectively, which were more than 50–100% of the mean observed snow depth.

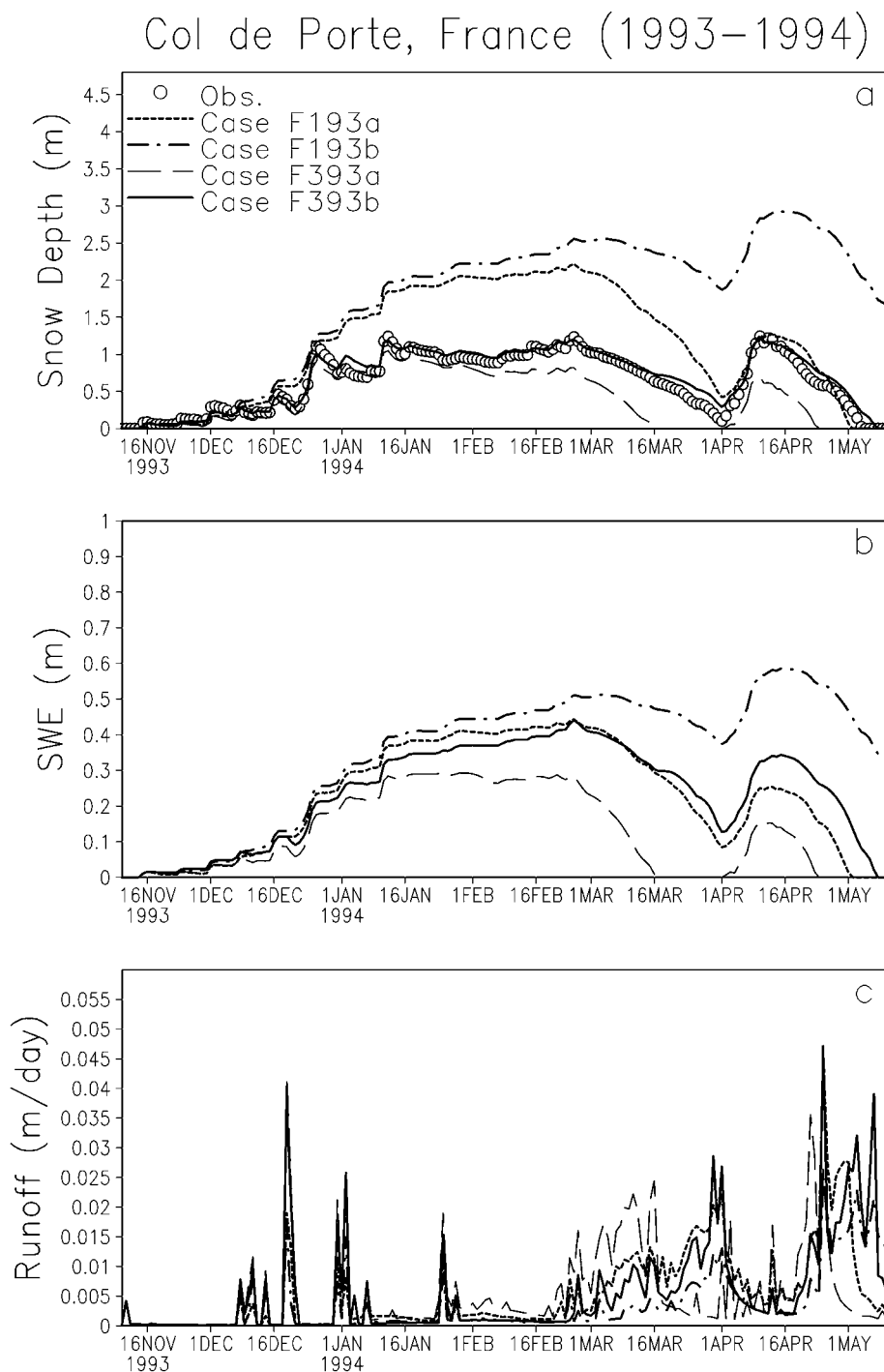


**Figure 4.** Simulated results for Cases F193a,b, and F393a,b for one winter season at Col de Porte: (a) total snow depth (m) along with the snow observations; (b) SWE (m); (c) runoff; (d) surface air temperature along with the observations ( $^{\circ}\text{C}$ ).

[27] The snow depth in Case F393a simulated the melting and refreezing episodes in the accumulation period. Compared with Case F193a, the simulated snow depth was reduced substantially, with the RMS being only 0.30 m, but it had a slightly lower correlation coefficient, 0.87, with the observational data. Still, Case F393a also had obvious deficiencies in simulating the snow depth during January, February and March. The snow depth was too thin and the

snow melting was too fast due to unrealistic low albedo. Both the first snowmelt during March and the second snowmelt during April occurred about a half-month earlier than observed (Figure 4a). Case F393b, which set the fresh snow albedo at about 0.85 (Figure 3), produced the best results with the correlation being 0.98 and the RMS error being only 0.09m. The simulated snow depth followed the observation closely. The differences between Case F193a

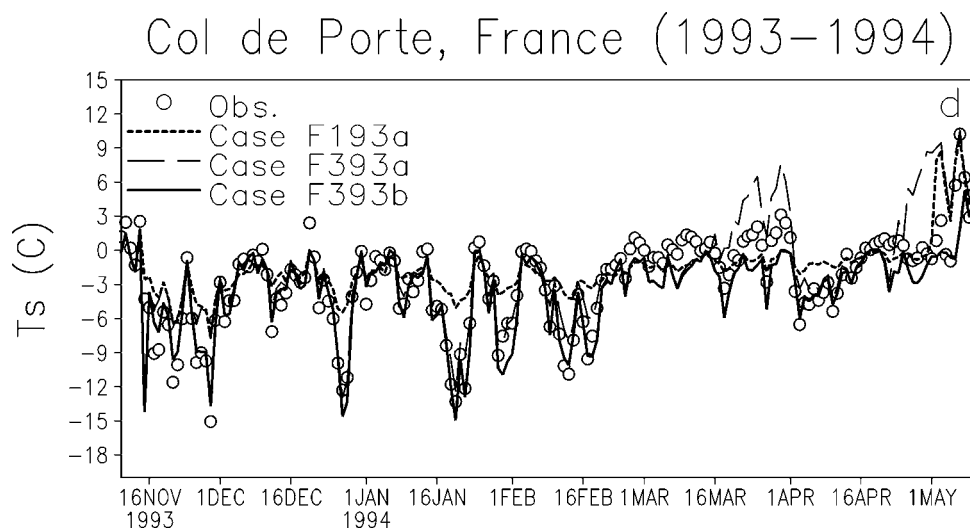


Figure 4. (continued)

and Case F193b and between Case F393a and Case F393b show the albedo effect, and the differences between Case F193a and Case F393a and Case F193b and Case F393b show the effect of other parameterizations. The correlation coefficients and the RMS errors for these three runs are listed in Table 1a.

[28] Consistent with the difference in snow depth, the effect of snow albedo and other parameterizations on SWE were also evident (Figure 4b), especially during the melting stage. According to *Boone and Etchevers*' [2001] Figure 3d, Case F393b's simulations (with multi-layer snow model and proper snow albedo) were close to measured SWE. Please note that in *Boone and Etchevers* [2001], the labels, such as "Jan," "Feb," in the figures, mean "Jan. 31," "Feb. 28." It is interesting to see that although the snow depths of Case F193 were quite different from Case F393, the SWE differences between Case F193a and Case F393b were, in fact, not that large. However, during the melting stage (after April 1), Case F193a still underestimated the SWE. For example, the observed maximum SWE in the middle of April was more than 0.3 m, while SWE in F193a was only 0.25m.

[29] The snow compaction played a major role in the differences in the simulated snow cover. This effect becomes evident only after late December when the snow depth reaches around 1m. After the first significant snow melting in late March, the snow depths in Case F193 and Case F393 were close again during the accumulation. But the effect of compaction in the second snow-melting period was still very clear. There are three mechanisms in the 3-Layer model that control the compaction as described in the last section. Our sensitivity study revealed that

destructive metamorphism and densification processes were dominant in Case F393 (not shown).

[30] All these four cases produced several intermittent strong runoffs during the accumulation period, large runoff during the first melting period, and very strong snow melting during the last melting period (Figure 4c). Case F193b produced extremely low runoff because most snow was still not melted at the end of the time period of integration (Figure 4b). The simulated timing and magnitudes of runoff were quite different between these cases. Case F393 in general produced more variability compared with Case F193 (Figure 4c). Case F393's peak runoffs were large. The surface snow layer of the model was quite thin in the 3-Layer model (only 2cm). This made the model more sensitive to the variability of the surface water and energy balance. Higher albedo in Case F393b also delayed the major runoff during the melting period for about a half-month compared with Case F393a, which was consistent with the delay in snow melting as shown in Figures 4a and 4b. However, it did not affect the timing of the runoff in the snow-accumulating period, only the amplitude.

[31] The surface energy balance was also sensitive to the snow parameterizations. In Case F193a, surface temperature had less variability (Figure 4d) and was close to the freezing point during most of the simulation because the snow pack was treated as a large bulk. The results in Case F193b were very similar to Case F193a but slightly cooler due to high albedo (not shown). In Cases F393, simulated temperature showed large variations because the surface snow layer was rather thin. Figure 4d shows that the simulations followed the observed variability quite well, at temperatures some-

Table 1a. Comparison of Observed and Simulated Snow Depth for the Col de Porte Site

Cases	Correlation	RMS, m	Case	Correlation	RMS, m
Case F193a	0.91	0.64	Case F393a	0.87	0.30
Case F193b	0.67	1.33	Case F393b	0.98	0.09
Case F188	0.84	0.22	Case F388	0.85	0.13
Case F194	0.88	0.41	Case F394	0.99	0.14
Case G1	0.55	0.43	Case G3	0.90	0.14

Table 1b. Comparison of Observed and Simulated Surface Temperature for the Col de Porte Site

Cases	Correlation	RMS, °K	Case	Correlation	RMS, °K
Case F193a	0.52	4.0	Case F393a	0.60	3.9
Case F193b	0.46	4.2	Case F393b	0.66	3.9
Case F188	0.72	2.9	Case F388	0.91	2.3
Case F194	0.84	2.6	Case F394	0.91	3.0

times as low as  $-15^{\circ}\text{C}$  (Figure 4d). The correlation coefficients were 0.52, 0.46, 0.60, and 0.66, for Cases F193a, F193b, F393a, and F393b, respectively, which indicated that the multi-layer model was able to capture the variability much better, but the RMS errors for the four cases were in a similar range (Table 1b). Case F393b has a cold bias. We suspect that the observational error might contribute to this bias. The observed temperature was higher than  $0^{\circ}\text{C}$  under the condition of low snow depth. However, the modeled temperature remained at or below freezing as long as snow existed (Figures 4a and 4d). The average surface temperatures for observation, Cases F193a, F193b, F393a, and F393b before March 1 were 268.9, 270.6, 270.1, 269.6, and 268.5, respectively. Between March 1 and May 1, when the major melting started, the average surface temperatures for observation, Cases F193a, F193b, F393a, and F393b were 272.4, 272.2, 271.7, 273.8, and 271.1, respectively. In Case F193a, the low snow albedo led to an early complete snow melting (Figure 4a) and higher surface temperature, which helped produce results close to observations during the snow-melting season. *Essery et al.* [1999] pointed out that the observed snow-surface temperature was possibly overestimated because of instrumentation being incorporated into the field of view of the radiation sensor, which was used to derive the surface temperature. This problem seems to be more apparent during the melting period. Apparently, in this case, the measured variability was likely more reliable than the absolute values.

[32] The study above showed that the 1-layer model needed tuned albedo to get better results. Because the albedo effects were so dominant in the cases discussed above and this parameter is relatively easy to be tuned should we have sites for calibration, in the further experiments, we applied the realistic fresh snow albedo in Case F393b for the 3-Layer model and the tuned albedo in Case F193a for the 1-Layer model, respectively, to the 1988–1989 and 1994–1995 data for simulations. Thus, these experiments would compare the best cases for each model and would test the necessity for more complex snow schemes rather than tuning the albedo. The results from the 3-layer model runs for these two years are referred to as Case F388 and Case F394, respectively, and the results from 1-Layer model runs are referred to as Case F188 and F194, respectively. The results from Case F188, F194, F388, and F394 were consistent with those discussed in Case F193 and Case F393 and are listed in Table 1a. For example, the simulated SWE in Case 194 and Case 394 were similar during the accumulation period and very different during the ablation period. Persistent snow melting in Case F194 started from about March 10, and the snow was completely melted around April 20. In Case F394, the snow melting started around April 1 and ended May 5 (Not shown). The SWE in Case 394 was more close to observation (based on Figure 3e in *Boone and Etchevers* [2001]), while Case F194 again underestimated the SWE as in Case F193. The 1994–1995 data set included measurements for the runoff. Case F394 produced much better correlation and smaller RMS than case F194 (Table 1c). The average observed runoff over this time period was  $9.5\text{mm day}^{-1}$ . The 1-Layer model significantly underestimated the runoff variability.

[33] The means of Case F188, F193b, and F194 and of Case F388, F393b, and F394 are referred to as Case F1 and

**Table 1c.** Comparison of Observed and Simulated Runoff for the Col de Porte Site

Cases	Correlation	RMS, mm
Case F194	0.52	12.4
Case F394	0.78	9.3

Case F3, respectively. The simulations of snow depth, SWE, and surface temperature of Cases F1 and Cases F3 are shown in Figure 5. Case F3's simulation was very close to the observation. Case F1 overestimated the snow depth during the snow accumulation period (snow density was too low) and underestimated the snow depth during the melting period, which then led to an early melting. Despite the large difference in snow depth, the difference in SWE was not that dramatic before the major snow melting kicked in (around March 1). Based on the available data for 1993–1994 and 1994–1995 as discussed before, Case F1's estimation was very likely underestimated. In addition, Case F3 produced better variability of the surface temperature during all three years (Table 1b). However, surface temperature in Case F1 was more close to observation during March and April. As discussed earlier, a number of investigators who used this data set have noted the higher bias in observational temperature [*Essery et al.*, 1999; *Boone and Etchevers*, 2001]. For example, from April 1, 1995 to May 15, 1995, the observed snow depth decreased from 1.5m to 0 yet the measured temperature was always above  $0^{\circ}\text{C}$  with a mean about  $3^{\circ}\text{C}$ . *Boone and Etchevers* [2001] just set the surface temperature to 0 when snow cover existed. In our study, due to lower snow albedo Case F1 had an earlier melting and its temperature became more close to the actual observation.

[34] Different snow parameterizations also produced different surface energy partitioning. Figures 6a, 6b, and 6c show the mean latent heat, sensible heat, and ground heat fluxes, respectively, for Case F1 and Case F3. During snow accumulation, the latent heat and sensible heat fluxes and their differences between F1 and F3 were small. The main differences were in the ground heat fluxes, which were consistent with the differences in surface temperature. After snow melting, the differences in latent heat and sensible heat fluxes between these two parameterizations became large. The averages of these fluxes before/after March 6, when the major snow melting started, are listed in Table 2. It should be pointed out that the results in this study were obtained from an off-line test. Under interactive conditions, the differences in surface fluxes between these two parameterizations could be larger and produce substantial feedback.

[35] To further confirm the discoveries in the Col de Porte site, we also tested the Gander data, which cover September 1, 1986 to May 31, 1987, September 1, 1987 to May 31, 1988, September 1, 1988 to May 31, 1989, and September 1, 1989 to May 30, 1990. The results from the 1-Layer model and the 3-Layer model are referred to as Case G1 and Case G3, respectively. Again, the sensitivity study showed the snow albedo was very important for proper simulation. In this area, we found that the best results were obtained when the fresh snow albedo was set to 0.75 in Case G3. Figure 7 shows the four-year mean snow depth from observation and simulation. The statistics

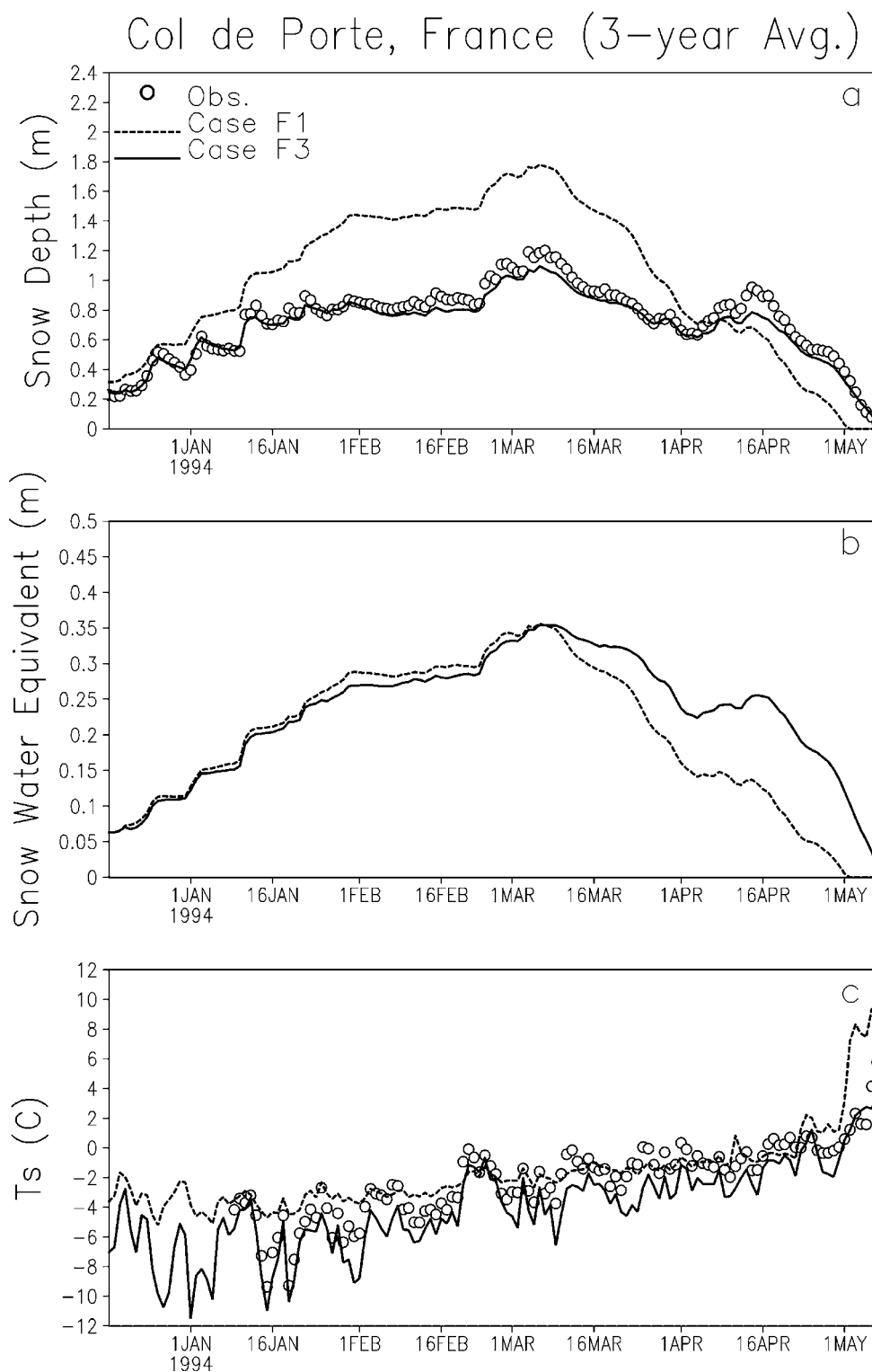


**Figure 5.** Simulated results and observation for three winter means at Col de Porte: (a) snow depth (m); (b) SWE (m); (c) surface air temperature (C°).

for the snow depth simulation are also listed in Table 1a. In general, Case G3 produced better results. The 1-Layer model showed much less variation (Table 1c). However, during the accumulation period, Case G3 simulated less snow depth, which indicated the compaction rate in Case G3 may be too high since Case G1 and Case G3 had similar

SWE during that period. In this relatively low snow case (the SWE had a maximum of only 0.1m), despite the relatively higher fresh snow albedo (0.75 in Case G3 versus 0.6 in Case G1), the snow melting period in Case G3 was about one month earlier than in Case G1. The results from Case G3 and Case G1 again confirm the results from the

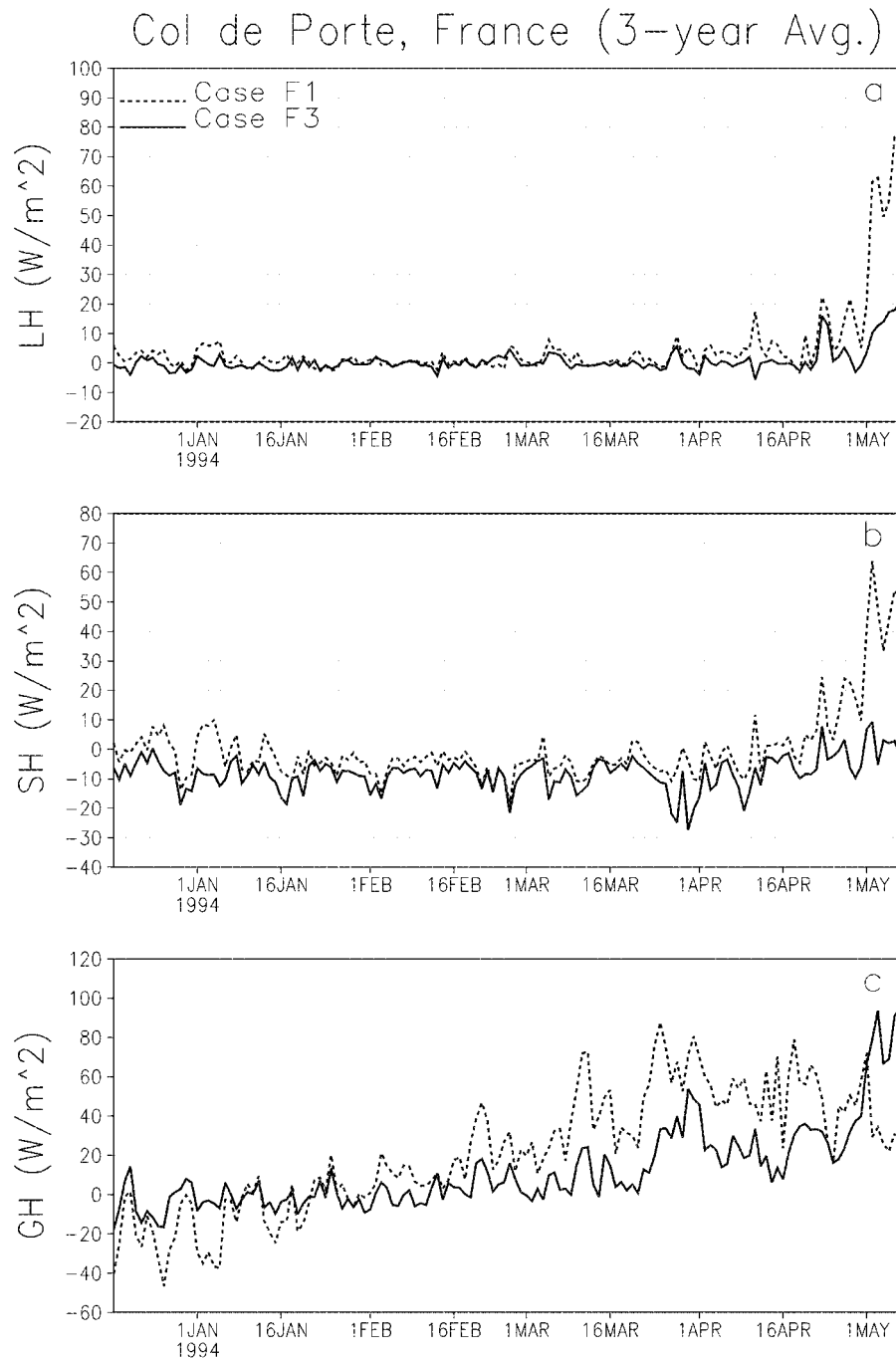


**Figure 6.** Simulated results for three winter means at Col de Porte: (a) latent heat flux ( $w m^{-2}$ ); (b) sensible heat flux ( $w m^{-2}$ ); (c) ground heat flux ( $w m^{-2}$ ).

French data: that snow layering and compaction, as well as snow albedo, were crucial for proper snow simulations.

#### 4.2. Testing Using the Ovre Lansjarv Data Set

[36] The Ovre Lansjarv data set was provided by the PILPS-2e project to calibrate snow models for the Torne/Kalix River system. During the calibration processes, we conducted a number of sensitivity studies to investigate the influence of parameters and parameterizations of the surface

model and the vegetation distribution on snow simulations. Since snow layering and compaction have been extensively tested in the previous section, they will not be further discussed in this section. We will mainly examine the effects of atmospheric stability, land cover conditions, and snow albedo during the melting period on the 3-Layer model simulation. The river discharge (runoff times basin area,  $m^3 sec^{-1}$ ) was the only data available for validation. In this study, we ran the model for twenty years and only

**Table 2.** Comparison of Simulated Fluxes Between Cases F1 and F3 for the Col de Porte Site ( $\text{w m}^{-2}$ )

	Before March 6		After March 6	
	Case F1	Case F3	Case F1	Case F3
Latent heat	1.1	-0.3	10.2	1.8
Sensible heat	-3.3	-8.9	5.0	-7.2
Ground heat	0.6	-0.4	49	28

present the results for the last ten years' simulation, as requested by the PILPS-2e experiment.

#### 4.2.1. Impact of Parameters and Parameterizations

[37] We have conducted very extensive tests to examine the sensitivity of snow simulations to the parameterizations and parameters using the Ovre Lansjarv data. Among these tests, it was found that two factors (aerodynamic resistance and snow albedo during the melting season) played a crucial role in proper runoff simulation. From flux measurements in Antarctica [King and Anderson, 1994], it was also found that the estimation of the turbulent fluxes was rather uncertain in the case of high stability and low wind-speed. Martin and Lejeune [1998] further found that the Deardorf's parameterization of the turbulent flux was underestimated during the stable condition under snow conditions.

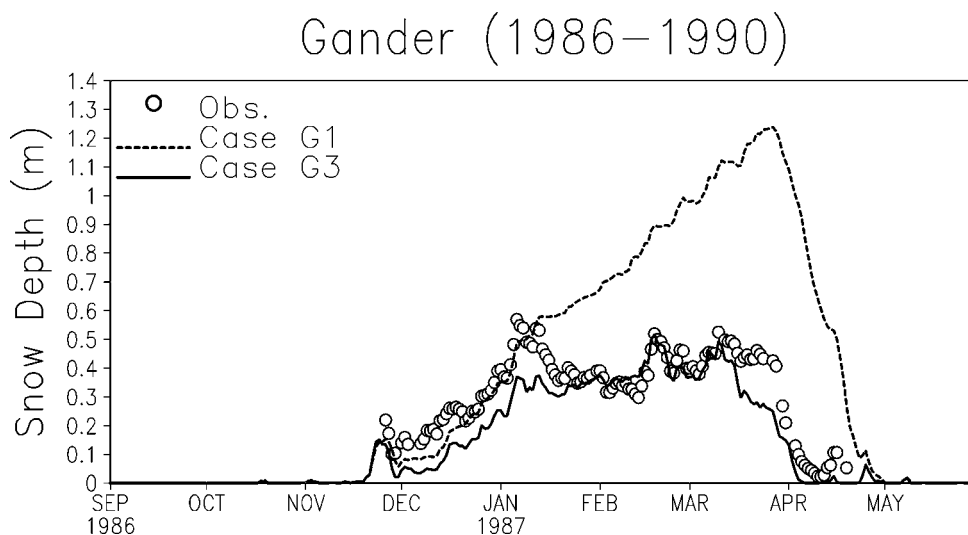
[38] In this section, we mainly present the results from the experiments that tested two factors mentioned above. Figure 8a shows the simulated ten-year mean discharge from the 3-Layer model simulations (referred to as Case L1). Although the general temporal variation in Case L1 was close to the observed pattern (a large peak during the snow melting and the second maximum during the summer), Case L1 produced too much runoff and an early runoff peak (about 10 days). Since soil moisture had no substantial variations during the winter season, higher runoff indicated a relatively lower evaporation.

[39] As discussed in section 2.1, the SSiB's aerodynamic resistance was derived based on Paulson's [1970] parameterizations, which, although tested by numerous experiments

and able to produce reasonable results in the French case, were not validated under rigid polar conditions. Because atmospheric conditions were rather stable during the polar winter, we suspected that the parameterization of the aerodynamic resistance in the stable condition might be responsible for the underestimation of the evaporation and then the overestimation of the runoff. Due to lack of measurements of the eddy transfer in the polar winter, as a sensitivity test we just ignored the non-neutral adjustment,  $C_{TT}^{-1}$ , in equations (1) and (2). This change would reduce the aerodynamic resistance in the stable regime. We refer to this experiment as Case L2.

[40] As expected, Case L2 enhanced the evaporation. This increase is especially large during the winter. From November through April, Case L2 produced  $4.5 \text{ w m}^{-2}$  more latent heat flux (Figure 9a, please note that the lines for Case L2 and Case L4 are often overlapped). In the meantime, the sensible heat flux was reduced by  $8 \text{ w m}^{-2}$  during the same time period (Figure 9b). The changes in heat fluxes led to lower snow depth (Figure 9c) and lower runoff. The average reduction of the snow depth was about 0.1m from January to May. Figure 8b shows the simulated discharge for Case L2. The average reduction in Case L2 was about  $2 \text{ m}^3 \text{ s}^{-1}$ , 11% of the simulated discharge in Case L1. The runoff simulation in the summer season was also changed, although it was not as dramatic as during the spring. However, the shift of the runoff peak in spring still existed. The correlation coefficient between the simulation and the observation was 0.88; actually it was slightly lower than the coefficient in Case L1, 0.91.

[41] This peak shifting occurred during the melting process, in which the snow albedo became lower. In SSiB, the albedo was empirically adjusted to 60% of the fresh snow albedo. Since this adjustment has not been validated by observational data, we designed a test to investigate the possible impact of this adjustment. In the test of the 3-Layer model referred to Case L3, we changed the adjustment to 90%, i.e. the snow had higher albedo during the melting season than in Case L1.

**Figure 7.** Simulated and observed three-year means of total snow depth (m) at Gander.

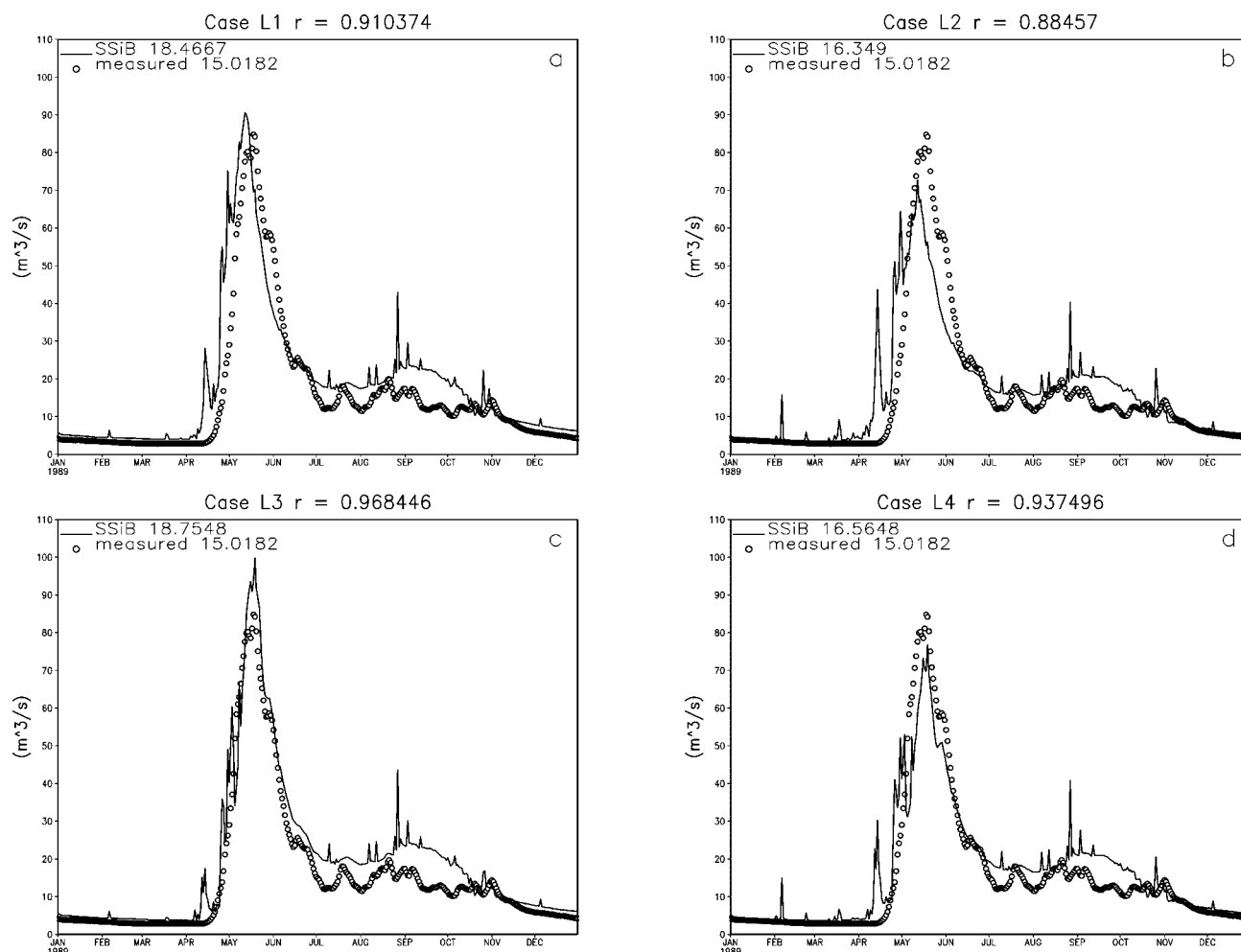


**Figure 8.** Simulated and observed discharge ( $\text{m}^3 \text{s}^{-1}$ ) for Ovre Lansjarv: (a) Case L1; (b) Case L2; (c) Case L3; (d) Case L4.

[42] Figures 9a and 9b show that Cases L1 and L3 had almost identical evaporation and sensible heat flux except during the spring melting season, in which Case L3 had lower evaporation and lower sensible heat flux. The snow depth became higher during that period. These changes postponed the runoff peak and were more consistent with the observations (Figure 8c). The correlation coefficient between simulation and observation was rather high, 0.97, but the simulated total runoff amount was too high.

[43] Because either Case L2 or Case L3 only solved one problem from Case L1, we conducted another test, Case L4, in which we included both changes from Cases L2 and L3. Figure 8d shows that Case L4 produced the best results with the proper runoff peak timing and the total runoff amount. But the spring peak was still lower and the summer maximum was still higher. The correlation coefficient between the simulation and observation was 0.94. Case L2 is just a sensitivity test and more proper parameterization for the aerodynamic resistance is necessary but pending on the observational data available.

[44] The combined effect of Case L2 and Case L3 were quite linear. The difference of the total discharge between Case L4 and Case L1 ( $-1.9 \text{ m}^3 \text{ s}^{-1}$ ) was close to the sum of the difference between Case L2 and Case L1 ( $-2.1 \text{ m}^3 \text{ s}^{-1}$ )

and the difference between Case L3 and Case L1 ( $0.3 \text{ m}^3 \text{ s}^{-1}$ ). The simulations of the snow depth and the heat fluxes in Case L4 generally followed that in Case L2 (Figure 9). Only during the snow melting season were the simulations in Case L4 between those in Case L2 and Case L3. The correlation coefficients and the mean discharge for these four cases are listed in Figure 8.

[45] The information obtained from this calibration study was applied to the PILPS-2e experiment for the entire Torne/Kalix River system. *Bowling et al.* [2003] and *Nijssen et al.* [2002] have comprehensively analyzed different models' (including SSiB) performance in the Torne/Kalix River basin.

#### 4.2.2. Impact of Vegetation Cover

[46] The Ovre Lansjarv site consists of woodland (71.7%), evergreen trees (2.3%), wooded grassland (25.6%), and water surface (only 0.4%). The results discussed in the last section took into account the land surface heterogeneity. The model simulated the runoff, snow depth, and fluxes for each land cover first. The average was then calculated based on the percentage coverage of each type. To test the effect of vegetation cover on the runoff and snow depth simulation, we conducted three tests: in one test, only woodland, i.e., the dominant vegetation type, was used to specify the land

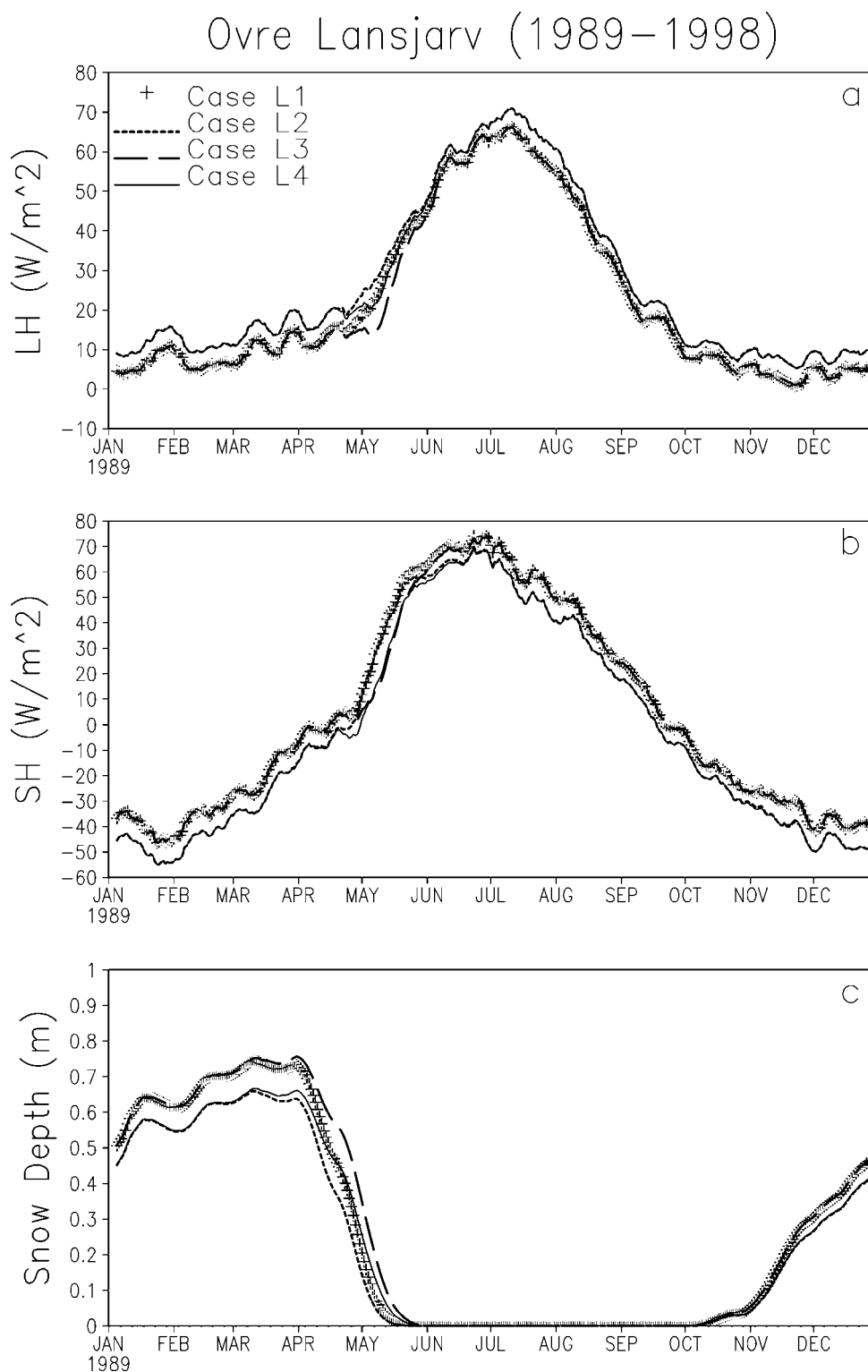


**Figure 9.** Simulated results for Cases L1, L2, L3, and L4: (a) latent heat flux ( $w m^{-2}$ ); (b) sensible heat flux ( $w m^{-2}$ ); (c) snow depth (m).

cover (referred to as Case L5); in the second test, wooded grassland was used to specify the land cover (referred to as Case L6); in the third test, only bare soil was assigned for the land cover (referred to as Case L7). The major vegetation parameters for woodlands and wooded grasslands are listed in Table 3.

[47] Case L6 produced more latent heat flux but less sensible heat flux than Case L5 (Figures 10a and 10b). Although woodlands produced slightly higher ( $2.4 w m^{-2}$ ) snow evaporation from the canopy, wooded grasslands generated higher snow evaporation ( $8.3 w m^{-2}$ ) from the ground during the winter and higher transpiration

**Table 3.** Vegetation Parameters for the Ovre Lansjarv Site

	Woodland	Woodgrass
LAI		
Winter	0.424	0.366
Spring	0.830	0.804
Summer	2.067	2.183
Autumn	0.458	0.329
Fractional vegetation cover	0.95	0.95
Roughness length, m	1.00	0.15
Landcover height, m	10	1.5
Soil hydraulic conductivity (m/s)	3.47E-05	3.47E-05
Total soil depth (m)	3.5	1.49

(by  $5.4 \text{ w m}^{-2}$ ) during the summer. The snow depth in Case L6 was less than in Case L5, but the variability in these two cases was very similar (Figure 11a). Despite the lower total annual discharge rate in Case L6,  $16.5 \text{ m}^3 \text{ s}^{-1}$  versus  $19.2 \text{ m}^3 \text{ s}^{-1}$  in Case L5, the peak discharge for wooded grasslands was much higher,  $140 \text{ m}^3 \text{ s}^{-1}$  versus  $96 \text{ m}^3 \text{ s}^{-1}$ , due to less capacity for the soil to hold the water (Figure 11b, Table 4). The timing of the peak in Case L6 was about one month earlier than in Case L5. While Case L6

generated the peak runoff during the melting season (late April to early May), Case L5 produced the peak after the melting (late May).

[48] Case L7 can be considered as a deforestation case. It had lower evaporation over the year compared with Cases L5 and L6 (Figure 10a). In particular, the downward sensible heat flux was much less than vegetated surface during the winter season. Snow depth was higher (Figure 11c) and so was the annual mean discharge ( $22.1 \text{ m}^3 \text{ s}^{-1}$ ). The discharge peak was extremely high, about  $220 \text{ m}^3 \text{ s}^{-1}$ , which was 57% and 129% more than in Cases L6 and L5, respectively. In addition, Case L7 also produced many mini-peaks during the summer rainy season. High runoff after deforestation has been observed in many locations in cold regions. For example, it was found that flooding was much enhanced in the European Alps in the last century, after deforestation [Goudie, 2000]. For comparison, the results from Case L1 were also shown in Figure 11. For this site with only two main vegetation types, the results from the area average and the dominant type are close; for example, the annual runoff difference was only about 4%. However, if the vegetation types were more diverse, based

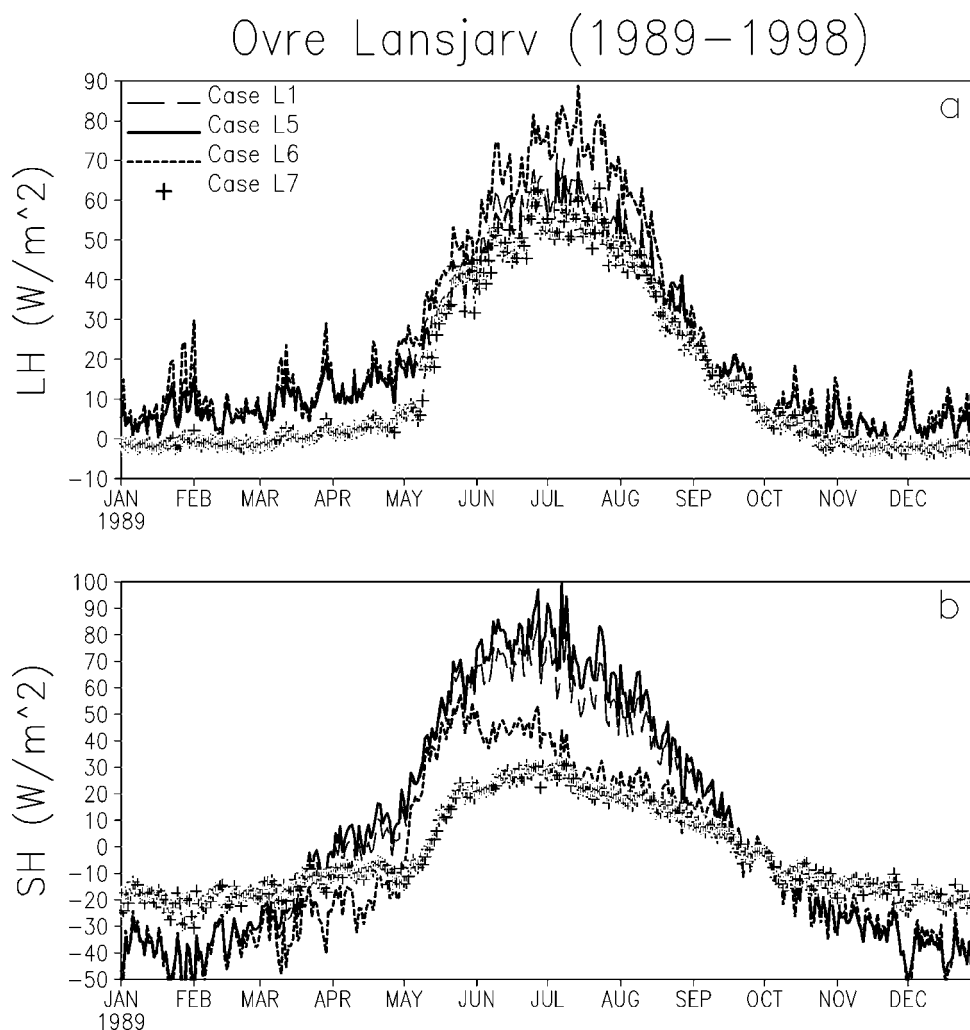


**Figure 10.** Simulated results for Cases L1, L5, L6, and L7: (a) latent heat flux ( $\text{w m}^{-2}$ ); (b) sensible heat flux ( $\text{w m}^{-2}$ ).

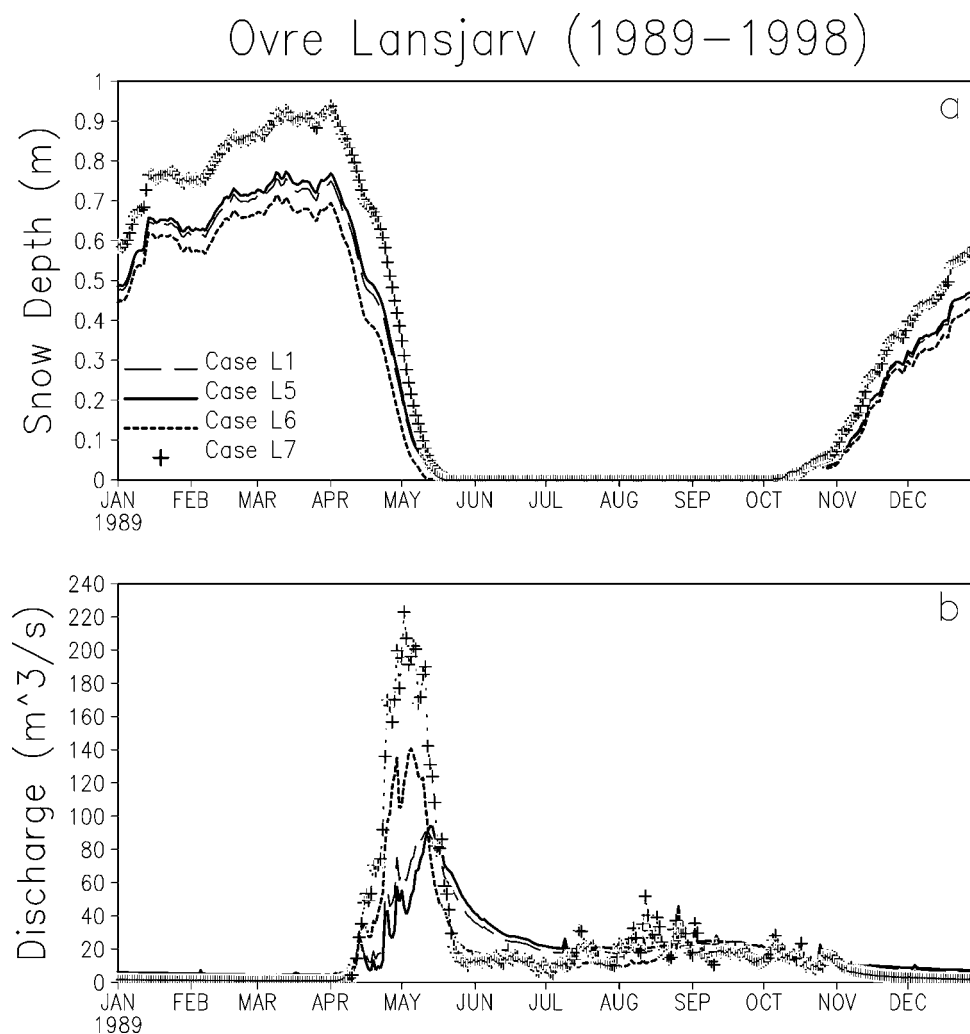


**Figure 11.** Simulated results for Cases L1, L5, L6, and L7: (a) snow depth (m); (b) discharge ( $\text{m}^3 \text{s}^{-1}$ ).

on the results from this section, selection of the dominant vegetation type as the area mean could produce large errors.

[49] Table 4 also shows that during the snow-covered period, vegetation enhanced downward sensible heat flux. With different vegetation types, the canopy-received sensible heat flux was almost the same, but the trees prevented more sensible heat flux from reaching the ground and influencing the snow melting. For the latent heat flux, bare soil produced very little evaporation. Trees produced more evaporation from the canopy but less evaporation from the ground compared with grassland.

## 5. Conclusion

[50] We designed a series of numerical experiments to understand the physics at the soil-vegetation-snow-atmosphere interface and to find the major parameterizations/parameters, which are crucial to simulate the cold season processes. Three observational data sets were used to help us interpret the results.

[51] The study shows that snow layering and compaction are important to simulate the snow depth and SWE during the ablation period. The 3-Layer model produced signifi-

cantly different SWE during the melting period from the 1-Layer model. Although the estimation of the snow depth in the 1-Layer Model during the accumulation period could probably be improved by assigning a better value for a constant snow density, its deficiency in the ablation period is inevitable. Many studies have shown the ablation period is crucial in determining the net variability in cold regions [Thompson, 1997]. The multiple snow layers, which imply a separation of the soil temperature and snow temperature, are necessary to properly simulate the variability of snow-covered surface temperature. With a bulk snow/soil layer, the surface temperature would persistently be close to the

**Table 4.** Simulated Mean Latent Heat and Sensible Heat Fluxes ( $\text{w m}^{-2}$ ) for the Ovre Lansjarv Site Between 1 November Through 30 April

Cases	Latent Heat Flux		Sensible Heat Flux	
	Ground	Canopy	Ground	Canopy
L1	5.5	2.1	-20.5	-6.8
L5	4.6	2.4	-19.3	-6.3
L6	8.3	0.6	-25.6	-6.6
L7	-0.5	0	-16.4	0

freezing point, and its variability is substantially hampered. Furthermore, the variability and the amplitude of the runoff during the snow-melting season could be severely underestimated in the 1-Layer Model. However, from the results in this study, the impact of layering and compaction on the surface fluxes during the snow accumulation period is rather limited.

[52] The snow albedo, including the albedo during the melting stage, is crucial for the simulations in all the cases discussed in this study. While the 1-Layer model requires relatively low snow albedo to produce reasonable simulations, the multi-layer model needs to have realistic snow albedo. When the albedo increases from about 0.65 to about 0.85, the timing for the completion of snow melting and the runoff peak could be delayed by about half a month. Meanwhile, the melting snow albedo alone could also affect the timing of the runoff peak. Although we could tune the snow albedo in an off-line test, in GCM or regional model studies, realistic snow albedo is necessary. Recent study showed that the snow albedo was scale dependent (Rachel Pinker of University of Maryland, personal communications, 2002). With the horizontal resolution less than 1/8 degree, the remotely sensed snow albedo is about 0.8–0.9. However, when the horizontal resolution reaches 2 degrees, the snow albedo becomes about 0.6–0.7. It is very likely the snow age, heterogeneity, and other factors play a role ([www.atmos.umd.edu/~srb/gcip](http://www.atmos.umd.edu/~srb/gcip)).

[53] The parameterization of the stability condition is another important issue in cold regions. The results from Cases L1–L4 clearly indicate that the surface energy partitioning is divided into two groups based on the parameterizations in the surface aerodynamic resistance. In this study, although the difference in this study is not as dramatic as the compaction, layering, and snow albedo, parameterization of surface aerodynamic resistance is also an important issue and there is so far no reliable data to better understand this issue.

[54] Our last sensitivity study shows that although the snow may fully cover the ground in cold regions during the winter, vegetation still exerts an important role in the cold region and cold season simulations. Less downward sensible heat flux over the bare ground produced thick snow cover and extremely high peak runoff, which is a typical deforestation scenario in cold regions.

## Appendix. Coupling Methodology

[55] The coupling methodology is crucial to ensure energy conservation at the vegetation-snow-soil interface [Xue *et al.*, 2001]. The changes in temperature and humidity in the vegetation/snow layer should be consistent with the flux exchange between these two layers. Although this principle is simple and well known, its realization is a rather difficult task. The SAST model only deals with the atmosphere-snow-soil continuum, and the direct interactive effect between vegetation and snow cover was not involved. When the snow cover is sandwiched between vegetation above and soil below in SSiB, the snow cover is directly interactive upwards with the vegetation layer and downwards with the soil surface. We briefly present the major coupling equations, and a detailed presentation can be found in Sun and Xue [2001].

[56] The governing equation for canopy temperature  $T_c$  is based on the energy conservation equation:

$$C_c \frac{\partial T_c}{\partial t} = R_{nc} - H_c - \lambda E_c \quad (A1)$$

where  $C_c$  ( $J m^{-2} K^{-1}$ ),  $R_{nc}$  ( $w m^2$ ),  $H_c$ , and  $\lambda E_c$  are heat capacity of canopy, net radiation, sensible heat, and latent heat fluxes at the canopy level, respectively. The budget equation of enthalpy for each snow layer is

$$\frac{\partial H(Z)}{\partial t} = \frac{\partial}{\partial Z} (G_{ns}(Z) - R_{sw}(Z)) \quad (A2)$$

where  $H$  ( $J m^{-3}$ ) and  $R_s$  ( $w m^2$ ) are the volumetric enthalpy of water and short wave radiation flux at snow layers, respectively.  $R_{sw}$  is calculated from equation (3).  $G_{ns}$  ( $w m^2$ ) is the heat flux through the snow layer.

$$G_{ns} = \begin{cases} R_{ns} - H_s - \lambda E_s + G_{pr} & \text{at the snow surface} \\ -K \frac{\partial T_s(Z)}{\partial Z} & \text{within snow layers} \end{cases} \quad (A3)$$

where  $K$  ( $W m^{-1} K^{-1}$ ),  $T_s$ ,  $R_{ns}$ ,  $H_s$ ,  $\lambda E_s$ ,  $G_{pr}$  are effective heat conductivity, snow temperature, net radiation, sensible heat, latent heat fluxes at the canopy level, and heat energy brought to the snow surface layer by precipitation, respectively. The force-restore method is used to predict the time variation of the ground temperature  $T_{gs}$ .

$$C_{gs} \frac{\partial T_{gs}}{\partial t} = G_{ns}(Z_1) - \frac{2\pi C_{gs}}{\tau} (T_{gs} - T_d) \quad (A4)$$

where  $C_{gs}$ ,  $T_d$ ,  $G_{ns}(Z)$ ,  $\tau$ ,  $Z_1$  are heat capacity of soil surface, deep soil temperature,  $G_{ns}$  at snow/soil interface, day length, and the snow layer at snow/soil interface, respectively. In the original SSiB, (A4) and (A1) are coupled together to ensure energy conservation. In SSiB and SAST coupling, the equations (A1) and (A2) are solved by an implicit backward method. Equation (A1) can be discretized as

$$C_c \frac{\Delta T_c}{\Delta t} = R_{nc} + \frac{\partial R_{nc}}{\partial T_c} \Delta T_c + \frac{\partial R_{nc}}{\partial T_{Z_3}} \Delta T(Z_3) - H_c - \frac{\partial H_c}{\partial T_c} \Delta T_c - \frac{\partial H_c}{\partial T_{Z_3}} \Delta T(Z_3) - \lambda E_c - \frac{\partial \lambda E_c}{\partial T_c} \Delta T_c - \frac{\partial \lambda E_c}{\partial T_{Z_3}} \Delta T(Z_3) \quad (A5)$$

where  $Z_3$  is the snow layer at snow/air interface,  $\Delta T_c = T_c^{(t+1)} - T_c^{(t)}$  and  $\Delta T(Z_3) = T(Z_3)^{(t+1)} - T(Z_3)^{(t)}$ . The temperature in the snow layers can be calculated by the following equation:

$$H = C_v \times (T - 273.16) - f_i \times L_{fi} \times W \times \rho_i \quad (A6)$$

where  $C_v$  is the mean snow volumetric specific heat capacity ( $J m^{-3} k^{-1}$ ),  $f_i$  is dry snow mass fraction of the total snow mass,  $L_{fi}$  is the latent heat of fusion for ice,  $W$  is the volumetric SWE, and  $\rho_i$  is the liquid water intrinsic

density. From (A6) and (A2) after some numerical manipulation, the numerical equation for (A2) at the top snow layer becomes

$$\begin{aligned} \frac{C_v \Delta T(Z_3) - L_{fi} W(Z_3) \rho_i \Delta f_i(Z_3)}{\Delta t} &= R_{nz3} + \frac{\partial R_{nz3}}{\partial T_c} \Delta T_c \\ &+ \frac{\partial R_{nz3}}{\partial T_{z_3}} \Delta T(Z_3) - H_{z_3} - \frac{\partial H_{z_3}}{\partial T_c} \Delta T_c \\ &- \frac{\partial H_{z_3}}{\partial T_{z_3}} \Delta T(Z_3) - \lambda E_{z_3} - \frac{\partial \lambda E_{z_3}}{\partial T_c} \Delta T_c + \frac{\partial \lambda E_{z_3}}{\partial T_{z_3}} \Delta T(Z_3) \\ &+ G_{pr} - C_{sn} \Delta T(Z_3) - C_{sn} (T^r(Z_3) - T(Z_2)) \end{aligned} \quad (A7)$$

where  $Z_2$  is the second snow layer,  $G_{pr}$  represents the enthalpy from the sum of rain or dry snow, and  $C_{sn}$  is the coefficient obtained during the derivation of Equation (A7). From Equations (A5) and (A7), the variables with fast changes, i.e., snow temperature and canopy temperature, are solved simultaneously. Because the changes of temperatures in the second and third snow layers, as well as in the soil layer, are relatively slow under snow insulation, a forward numerical scheme is adopted to obtain these temperatures.

[57] **Acknowledgments.** We are appreciative of Eric Martin of Météo-France Centre National de Recherches Météorologiques for providing the French snow data, Bettina Loth of the Max-Planck Institut Für Meteorologie for providing the Gander data, Rachel Pinker of the University of Maryland for providing the radiation data for Gander and helpful discussions, and Dennis Lettenmaier and Laura Bowling of the University of Washington for the PILPS-2e data. We would also like to thank Guo-Yue Niu of the University of Texas at Austin for his help in processing the PILPS-2e data and useful discussions. S. Sun and Y. Jiao worked on this project while at University of Maryland. Research funding was provided by NOAA grants NA16GP1581, NASA grants NAG5-9014, NSF EAR 9706403, and Chinese NSF 40233034 and CNSF40075019.

## References

- Anderson, E. A., A point energy and mass balance model of a snow cover, *NOAA Tech. Rep. NWS, 19*, Office of Hydrol., Natl. Weather Serv., Silver Spring, Md., 1976.
- Boone, A., and P. Etchevers, An intercomparison of three snow schemes of varying complexity coupled to the same land surface model: Local-scale evaluation at an Alpine site, *J. Hydrometeorol.*, *2*, 374–394, 2001.
- Bowling, L. C., et al., Simulation of high latitude hydrological processes in the Torne Kalix basin: PILPS phase 2(e): 1. Experiment description and summary inter-comparisons, *Global Planet. Change*, *38*, 1–30, 2003.
- Brun, E., P. David, M. Sudul, and G. Brunot, A numerical model to simulate snow cover stratigraphy for operational avalanche forecasting, *J. Glaciol.*, *38*, 13–22, 1992.
- Businger, J. A., J. C. Wyngaard, Y. I. Zumi, and E. G. Bradley, Flux-profile relationships in the atmosphere surface layer, *J. Atmos. Sci.*, *28*, 181–189, 1971.
- Carlson, B., Some facts about the Yorne and Kalix River Basins, *Hydrol. Rep. 80*, Swedish Meteorol. and Hydrol. Inst., Stockholm, Sweden, 1999.
- Cherkauer, K. A., and D. P. Lettenmaier, Hydrologic effects of frozen soils in the upper Mississippi River basin, *J. Geophys. Res.*, *104*, 19,599–19,610, 1999.
- Deardorff, J. W., Efficient prediction of a ground surface temperature and moisture with inclusion of a layer of vegetation, *J. Geophys. Res.*, *83*, 1889–1903, 1977.
- Dickinson, R. E., A. Henderson-Sellers, and K. J. Kennedy, Biosphere-Atmosphere Transfer Scheme (BATS) version 1e as coupled to the NCAR Community Climate Model, *NCAR Tech. Note NCAR/TN-387 + STR*, 72 pp., Nat. Cent. for Atmos. Res., Boulder, Colo., 1993.
- Dorman, J. L., and P. Sellers, A global climatology of albedo, roughness length and stomatal resistance for atmospheric general circulation models as represented by the Simple Biosphere Model (SiB), *J. Appl. Meteorol.*, *28*, 833–855, 1989.
- Douville, H., J. F. Royer, and J. F. Mahfouf, A new snow parameterization for the Meteo-France climate model: Part I. Validation in stand-alone experiments, *Clim. Dyn.*, *12*, 21–31, 1995.
- Essery, R., E. Martin, H. Douville, A. Fernández, and E. Brun, A comparison of four snow models using observations from an alpine site, *Climate Dyn.*, *15*, 583–593, 1999.
- Goudie, A., *The Human Impact on the Natural Environment*, 5th Ed., 511 pp., MIT Press, Cambridge, Mass., 2000.
- Henderson-Seller, A., Z.-L. Yang, and R. E. Dickinson, The project for Intercomparison of Land-surface Parameterization Schemes, *Bull. Am. Meteorol. Soc.*, *74*, 1335–1349, 1993.
- Jin, J. M., X. Gao, Z.-L. Yang, R. C. Bales, S. Sorooshian, R. E. Dickinson, S. F. Sun, and G. X. Wu, Comparative Analyses of physically based snowmelt models for climate simulations, *J. Clim.*, *12*, 2643–2657, 1999.
- Jordan, R., A One-dimensional temperature model for a snow cover, *Spec. Rep. 91-1b*, Cold Regions Res. and Eng. Lab., Hanover, N. H., 1991.
- Kalnay, E., et al., The NMC/NCAR 40-year reanalysis project, *Bull. Am. Meteorol. Soc.*, *77*, 437–471, 1996.
- King, J. C., and P. S. Anderson, Heat and Water vapour fluxes and scalar roughness length over an Antarctic ice shelf, *Boundary Layer Meteorol.*, *69*, 101–121, 1994.
- Lehnings, M., P. Bartlet, and B. Brown, Operational use of a snowpack model for the avalanche warning service in Switzerland: model development and first experiences, *Nor. Geotech. Inst.*, *203*, 169–174, 1998.
- Loth, B., and H. F. Graf, Snow cover model for global climate simulation, *J. Geophys. Res.*, *98*, 10,451–10,464, 1993.
- Loth, B., and H. F. Graf, Modeling the snow cover for climate studies, *Rep. 190*, 63 pp., Max-Planck-Institut für Meteorologie, Hamburg, 1996.
- Luo, L., et al., Effects of frozen soil on soil temperature, spring infiltration, and runoff: Results from the PILPS 2(d) experiment at Valdai, Russia, *J. Hydrometeorol.*, *4*, 334–351, 2003.
- Lynch, A. H., D. L. McGinnis, and D. A. Bailey, Snow-albedo feedback and the spring transition in a regional climate system model: Influence of land surface model, *J. Geophys. Res.*, *103*, 29,037–29,049, 1998.
- Lynch-Stieglitz, M., The development and validation of a simple snow model for the GISS GCM, *J. Clim.*, *7*, 1842–1855, 1994.
- Martin, E., and Y. Lejeune, Turbulent Fluxes above the snow surface, *Ann. Glaciol.*, *26*, 179–183, 1998.
- Mocko, D. G., G. Walker, and Y. Sud, New snow physics to complement SsiB: Part II. Effects on soil moisture initialization and simulated fluxes, precipitation and hydrology of GEOS II GCM, *J. Meteorol. Soc. Japan*, *77*, 349–366, 1999.
- Mocko, D., and Y. Sud, Refinements to SsiB with an emphasis on snow physics: evaluation and validation using GSWP and Valdai data, *Earth Interact.*, *5*, 2001. (Available at <http://EarthInteractions.org>)
- Niu, G.-Y., and Z.-L. Yang, The versatile integrator of surface atmospheric processes (VISA) Part 2: Evaluation of three topography-based runoff scheme, *Global Planet. Change*, *38*, 191–208, 2003.
- Nijssen, B., et al., Simulation of high latitude hydrological processes in the Torne Kalix basin: PILPS phase 2(e): 2. Comparison of model results with observations, *Global Planet. Change*, *38*, 31–53, 2002.
- Paulson, C. A., Mathematical representation of wind speed and temperature profiles in the unstable atmospheric surface layer, *J. Appl. Meteorol.*, *9*, 857–861, 1970.
- Peixoto, J. P., and A. H. Oort, *Physics of Climate*, 520 pp., Am. Inst. of Phys., New York, 1992.
- Pitman, A. J., Z.-L. Yang, J. G. Cogley, and A. Henderson-Sellers, Description of base essentials of surface transfer for the Bureau of Meteorology Research Centre AGCM, *Res. Rep. 32*, 117 pp., Bur. Of Meteorol. Res. Cent., Sydney, Aust., 1991.
- Pitman, A. J., A. G. Slater, C. E. Desborough, and M. Zhao, Uncertainty in the simulation of runoff due to the parameterization of frozen soil moisture using the global soil wetness project methodology, *J. Geophys. Res.*, *104*, 16,879–16,888, 1999.
- Robock, A., K. V. Vinnikov, C. A. Schlosser, N. A. Speranskaya, and Y. Xue, Use of Russian soil moisture and meteorological observations to validate soil moisture simulations with biosphere and bucket models, *J. Clim.*, *8*, 15–35, 1995.
- Schlosser, C. A., A. Robock, K. Y. Vinnikov, N. A. Speranskaya, and Y. Xue, 18-year land-surface hydrology model simulations for a midlatitude grassland catchment in Valdai, Russia, *Mon. Weather Rev.*, *125*, 3279–3296, 1997.
- Slater, A. G., et al., The representation of snow in land-surface schemes: Results from PILPS 2(d), *J. Hydrometeorol.*, *2*, 7–25, 2001.
- Stieglitz, M., A. Ducharme, R. Koster, and M. Suarez, The impact of detailed snow physics on the simulation of snow cover and subsurface thermodynamics at continental scales, *J. Hydrometeorol.*, *2*, 228–242, 2001.

- Sud, Y. C., and D. M. Mocko, Development and evaluation of a new snow-physics model to complement SSiB (Part I), *J. Meteorol. Soc. Jpn.*, 77, 335–348, 1998.
- Sun, S., and Y. Xue, Implementing a new snow scheme in Simplified Simple Biosphere Model (SSiB), *Adv. Atmos. Sci.*, 18, 335–354, 2001.
- Sun, S., J. M. Jin, and Y. Xue, A simplified layer snow model for global and regional studies, *J. Geophys. Res.*, 104, 19,587–19,597, 1999.
- Thompson, R. D., Glaciers, in *Applied Climatology: Principle and Practice*, edited by R. D. Thompson and A. Perry, pp. 74–88, Routledge, New York, 1997.
- Verseghy, D. L., Class-a Canadian land surface scheme for GCMs: 1. Soil model, *Int. J. Clim.*, 11, 111–133, 1991.
- Xue, Y., P. J. Sellers, J. L. Kinter III, and J. Shukla, A simplified biosphere model for global climate studies, *J. Clim.*, 4, 345–364, 1991.
- Xue, Y., H. G. Bastable, P. A. Dirmeyer, and P. J. Sellers, Sensitivity of simulated surface fluxes to changes in land surface parameterization: A study using ABRACOS data, *J. Appl. Meteorol.*, 35, 386–400, 1996a.
- Xue, Y., F. J. Zeng, and C. A. Schlosser, SSiB and its sensitivity to soil properties: A case study using HAPEX-Mobilhy data, *Global Planet. Change*, 13, 183–194, 1996b.
- Xue, Y., P. J. Sellers, F. J. Zeng, and C. A. Schlosser, Comments on “Use of midlatitude soil moisture and meteorological observations to validate soil moisture simulations with biosphere and bucket models,” *J. Clim.* 10, 374–376, 1997.
- Xue, Y., F. J. Zeng, K. Mitchell, Z. Janjic, and E. Rogers, The impact of land surface processes on the simulation of the U.S. hydrological cycle: A case study of 1993 US flood using the Eta/SSiB regional model, *Mon. Weather Rev.*, 129, 2833–2860, 2001.
- Yang, Z. L., E. R. E. Dickinson, A. Robock, and K. Y. Vinikov, Validation of the snow submodel for biosphere-atmosphere transfer scheme with Russian snow cover and meteorological observational data, *J. Clim.*, 10, 353–373, 1997.
- 
- Y. Jiao, University Quebec at Montreal, 550 Sherbrooke West Road, Montreal QC H3A 1B9, Canada.
- D. S. Kahan and Y. Xue, Department of Geography, University of California, Los Angeles, 1255 Bunche Hall, Los Angeles, CA 90095, USA. (yxue@geog.ucla.edu)
- S. Sun, The Institute of Atmospheric Sciences, Chinese Academy of Sciences, P.O. Box 9804, Beijing 100029, China.